Available online at www.sciencedirect.com
SCIENCE DIRECT
Thermochimica Acta 444 (2006) 117–127
thermochimica acta
www.elsevier.com/locate/tca

Dependence of size and size distribution on reactivity of aluminum nanoparticles in reactions with oxygen and MoO_3

Juan Sun [a], Michelle L. Pantoya [b], Sindee L. Simon [a,*]

[a] *Department of Chemical Engineering, Texas Tech University, Lubbock, TX 79409, United States*
[b] *Department of Mechanical Engineering, Texas Tech University, Lubbock, TX 79409, United States*

Received 28 August 2005; received in revised form 28 February 2006; accepted 2 March 2006
Available online 18 April 2006

Abstract

The oxidation reaction of aluminum nanoparticles with oxygen gas and the thermal behavior of a metastable intermolecular composite (MIC) composed of the aluminum nanoparticles and molybdenum trioxide are studied with differential scanning calorimetry (DSC) as a function of the size and size distribution of the aluminum particles. Both broad and narrow size distributions have been investigated with aluminum particle sizes ranging from 30 to 160 nm; comparisons are also made to the behavior of micrometer-size particles. Several parameters have been used to characterize the reactivity of aluminum nanoparticles, including the fraction of aluminum that reacts prior to aluminum melting, heat of reaction, onset and peak temperatures, and maximum reaction rates. The results indicate that the reactivity of aluminum nanoparticles is significantly higher than that of the micrometer-size samples, but depending on the measure of reactivity, it may also depend strongly on the size distribution. The isoconversional method was used to calculate the apparent activation energy, and the values obtained for both the Al/O_2 and Al/MoO_3 reaction are in the range of 200–300 kJ/mol.

Keywords: Aluminum nanoparticles; MIC thermite reaction; Oxidation; MoO_3; DSC

1. Introduction

The thermal behavior of nanoparticles is known to differ from that in the bulk state due to their increased surface-area-to-volume ratio [1]. For example, small particles have lower melting points than bulk material because of the increased proportion of loosely bound surface atoms [1]. Although the melting point depression can be as great as 500 K for gold particles of 1 nm radius [2], the depression is relatively small for aluminum nanoparticles; for example, a depression of only 13 K is observed for a particle having a 10 nm radius aluminum core with a passivation layer of approximately 10 nm [3].

In terms of reactivity, aluminum nanoparticles are more reactive than their micrometer-sized counterparts and their reactivity is found to depend on particle size, as well as on the type and thickness of the passivation layer [4–7]. For example, the reaction onset temperature measured in differential scanning calorimetry (DSC) is lower for aluminum nanoparticles in both air, oxygen, and nitrogen environments compared with those for micrometer-sized particles [4]. In addition, the onset temperature for oxidation of aluminum nanoparticles in air, as measured by thermogravimetric analysis (TGA), decreases with decreasing particle size [5,6] and is found to also depend on the type and thickness of the passivation layer [5]. Agglomeration of aluminum nanoparticles, on the other hand, decreases their reactivity in air [7], and although high-melting point passivation layers are said to reduce agglomeration [8], agglomeration has been found to occur in spite of the presence of a passivating layer [9]. In addition to reactivity in various gaseous environments, the activation energy for the oxidation of aluminum nanoparticles has been reported. Jones et al. used various thermal analysis techniques to obtain the activation energy for oxidation of Alex aluminum powder in air and reported values that ranged from 206 to 225 kJ/mol [10], whereas for a smaller diameter aluminum powder, Aumann found E_a to be 48 kJ/mol below 375 °C and 164 kJ/mol above that temperature [11], the latter of which was reported to be the same as that for oxidation of flat aluminum samples. Tompa et al. compared the oxidation of 100 and 900 nm

* Corresponding author.
E-mail address: sindee.simon@ttu.edu (S.L. Simon).

0040-6031/$ – see front matter © 2006 Elsevier B.V. All rights reserved.
doi:10.1016/j.tca.2006.03.001

aluminum nanoparticles in air using DSC and TGA and found activation energies of 243 and 264 kJ/mol for the smaller particles and values of 394 and 364 kJ/mol for the larger particles [12]. In addition to higher reactivity in air and nitrogen compared to their micrometer-sized counterparts, aluminum nanoparticles are also very sensitive to humidity, with complete oxidation of particles less than 90 nm diameter occurring in 74 days at 90% humidity [13].

Due to their high mass caloricity, high reactivity, and the non-toxic nature of the reaction products, aluminum nanoparticles have been used to add energy and increase temperatures in conventional explosives and propellants. Jones et al. have found that adding aluminum nanoparticles to conventional explosives, such as TNT and RDX, generally lowers the reaction onset temperature and increases reaction rates [5,10]. Similar results were reported by Brousseau and Anderson for TNT [14] although reductions in detonation velocity were found in other systems after adding aluminum nanoparticles [14,15]. Dokhan et al. also found an increase in the burn rate for ammonium perchlorate (AP) solid rocket propellant when adding aluminum having a bimodal aluminum particle size distribution and containing 20% nanometer Al [16].

Nanoparticles may also be components of a class of energetic thermite materials known as metastable intermolecular composites (MIC) which consist of a fuel, such as aluminum, and an oxidizer, generally a metallic oxide. Since nanoparticles approach molecular dimensions, intermixing of fuel and oxidizer nanocomponents enhances homogeneity over that of traditional micrometer-sized energetic materials. In addition, the increase of surface area of nanoparticles allows more fuel to be in contact with oxidizer, thereby reducing heat and mass diffusion effects [17]. Consequently, compared with conventional energetic materials, MIC materials have significantly higher energy density [18–20]. Work from Pantoya's group has recently shown that ignition times are two orders of magnitude lower for nanocomposites of aluminum and molybdenum trioxide than for analogous composites composed of micrometer-size aluminum, and that the nanocomposites show a corresponding decrease in ignition temperatures [20]. Similar results were found for Ni/Al thermite systems as a function of particle size [21].

Although studies have shown that particle size and production method do affect reactivity, the effect of particle size and size distribution for particles manufactured in the same way and for particles less than 100 nm has not been well documented. Furthermore, the mechanism and reaction kinetics controlling oxidation of MIC materials and the effect of particle size and size distribution on the MIC reaction need further investigation. These are important both for modeling oxidation behavior and for tailoring a composite for a specific application. The objectives of this study are, thus, to determine the effect of aluminum nanoparticle size and size distribution on the reactivity and kinetics of aluminum oxidation using differential scanning calorimetry. Although the reaction conditions in the DSC differ from those used in thermite applications where temperatures are significantly higher and reaction rates are orders of magnitude faster, the insights gained in this study are relevant for a complete understanding of the effects of particle size and size distribution on reactivity. The systems studied include aluminum nanoparticles under an oxygen atmosphere (25% oxygen in argon) and aluminum/molybdenum trioxide (Al/MoO_3) MIC mixtures under an argon atmosphere.

2. Experimental

2.1. Materials

Nanoscale aluminum particles were obtained from Technanogy (Irvine, CA), and 3 μm size aluminum particles (3–4.5 μm, 97.5% purity) were purchased from Alfa Aesar (Milwaukee, WI). The physical properties of the Al nanoparticles are listed in Table 1. Two size distributions were studied: a broad and narrow distribution. The average particle diameter and standard deviation were obtained from SEM images; a typical size distribution curve has been published [22]. Other characteristics, such as surface area and size distribution, of the nanopowders have been

Table 1
Properties of aluminum nanoparticles

Particle diameter (nm)	Standard deviation (nm)	Weight-average particle diameter (nm)	Al content (%)		Oxide layer thickness (nm)		$\Delta H_{m,T}$ (J/g_{Al})
			Supplier	Our measurement	Supplier[a]	Our measurement[a]	
Broad size distribution samples							
17	12[b]	31	38	33	2.2	2.5	292
25	21	51	54	47	2.2	2.7	300
52	42	105	74	59	2.5	4.1	320
76	56[b]	142	80	–	2.9	–	340
101	56	160	82	–	3.5	–	360
Narrow size distribution samples							
43	2	43	74	57	2.1	3.5	325
63	3	63	82	69	2.2	3.7	332
81	3	81	84	71	2.6	4.4	340
92	3	92	83	72	3.1	4.8	350

[a] Both supplier and our estimates of the oxide layer thickness are based on Eq. (1) assuming that the oxide layer is amorphous. The calculated thickness is on average 18% thinner if one assumes that the layer is crystalline.

[b] Estimated based on the average ratio of standard deviation to particle size of the other three broad size distribution samples.

reported [23]; similar data are available for the micrometer-size particles [24].

The average particle size obtained from SEM experiments reflects the number size distribution, whereas the heat flow response in DSC experiments corresponds to the weight distribution of the sample. Consequently, the number-average particle size is converted to weight-average size assuming that the particles have Gaussian distribution; the weight-average sizes are shown in Table 1. We note that although the log normal distribution has been used to describe the particle size distribution for particles generated using the same technique [9,11], the Gaussian distribution has been shown to describe the particle size distribution well for vapor-deposited indium nanoparticles [25], and the calculated active aluminum content of our particles is closer to the experimental values when we assume a Gaussian distribution than when we assume a log normal distribution [3]. Other researchers have also assumed a Gaussian distribution in their work to mathematically demonstrate the influence of size distribution on the oxidation wave speed [26]. For two of the particle sizes studied having broad distributions, the standard deviations are not available; to obtain the weight-average particle size we assumed that the ratio of the standard deviation to particle diameter for these samples was the same as for the other three broad size distributions for which the standard deviation is reported.

Pure aluminum is pyrophoric, and thus, each aluminum nanoparticle is passivated with a 2–4 nm Al_2O_3 layer to protect the particles from premature reaction. As the particle size decreases, the total percentage of Al_2O_3 increases and can become a considerable amount of the total powder. In Table 1, the aluminum content (Al content) refers to the amount of active aluminum present, i.e., that aluminum which is not in the form of Al_2O_3. The aluminum content was obtained from mass gain measurements using a TGA by the supplier and also by our measurements as described in a subsequent section. Based on the aluminum content and the particle size, the thickness of the oxide layer (t_{oxide}) can be calculated through a mass balance:

$$t_{oxide} = R_o \left[1 - \left(\frac{\rho_{Al_2O_3} c}{\rho_{Al} + c(\rho_{Al_2O_3} - \rho_{Al})} \right)^{1/3} \right] \quad (1)$$

where R_o is the total particle size (including the oxide layer), c is the fractional aluminum content, and $\rho_{Al_2O_3}$ (3.05 g/cm^3) [27] and ρ_{Al} (2.7 g/cm^3) [28] are the densities of amorphous aluminum oxide and aluminum at room temperature, respectively. The oxide layer is assumed to be amorphous based on the results of other researchers [24]; if the layer is assumed to be crystalline, its thickness is on average 43% thinner than reported in Table 1. Although our measurements show a lower aluminum content compared to those of the supplier, the aluminum content changes less than 3% during storage in our laboratory based on the results of TGA experiments conducted two months apart.

Molybdenum trioxide was obtained from Climax Molybdenum (Sahuarita, AZ) and is composed of rectangular sheet like particles approximately 1 μm in length and 20 nm thick. To make the MIC samples, an appropriate amount of aluminum and molybdenum trioxide were immersed in a solvent of hexanes and mixed using ultrasonic waves; no evidence of sintering is observed using our mixing method based on SEM measurements [29]. The solution was poured into a glass container and after the solvent was completely evaporated the mixture was carefully collected and put in a vial for further use. The equivalence ratio (ϕ) of aluminum to molybdenum trioxide is 1.2, where ϕ is defined as [30]:

$$\phi = \frac{(F/\mathrm{Ox})_{ACT}}{(F/\mathrm{Ox})_{ST}} \quad (2)$$

where F represents mass of fuel (Al), Ox the mass of oxidizer (MoO_3), and the subscripts ACT and ST indicate the actual and stoichiometric ratios. The stoichiometric F/Ox mass ratio for the reaction is 0.375 based on the following global reaction:

$$2Al + MoO_3 \rightarrow Al_2O_3 + Mo \quad (3)$$

The aluminum content as obtained from the supplier was used in determining ϕ. The equivalence ratio of 1.2 was found to be optimum for this reaction based on burn rate and ignition sensitivity studies [20]. The actual equivalence ratio based on the aluminum content obtained from our TGA measurements (which are described below) is shown in Table 2. Interestingly the actual equivalence ratio based on our measurements of the aluminum content ranges from 0.92 to 1.06 for the MIC samples studied with an average of 1.0, leading us to speculate that the optimum value of 1.2 found in earlier burn rate and ignition sensitivity studies [20] based on supplier values of aluminum content may in actuality be closer to 1.0 as might be expected from stoichiometric considerations. Also shown in Table 2 is the weight fraction of aluminum in the MIC samples (not including aluminum in the form of Al_2O_3).

2.2. Differential scanning calorimetry

Differential scanning calorimetry was performed using a Perkin-Elmer DSC-7 instrument with an ethylene glycol/water cooling system maintained at 10 °C. For the reaction of aluminum particles with oxygen, the runs were made under 25/75

Table 2
Properties of MIC samples

Al particle diameter (nm)	Weight-average particle diameter (nm)	Weight fraction aluminum in MIC samples	Actual ϕ
MICs with broad size distribution Al powders			
17	31	0.180	1.05
25	51	0.216	1.06
52	105	0.224	0.96
76	142	0.289	–
101	160	0.290	–
MICs with narrow size distribution Al powders			
43	43	0.214	0.92
63	63	0.243	1.00
81	81	0.255	1.02
92	92	0.254	1.05
MIC with bulk Al			
3000		0.308	1.20

oxygen/argon atmosphere; for the MIC reaction of aluminum particles with molybdenum trioxide, the runs were made under argon atmosphere. Alumina pans were used and sample sizes varied from 3 to 10 mg. Temperature scans were made as follows: the sample was held at 200 °C for 20 min for the Al/O_2 reaction and for 60 min for the MIC reaction to purge the sample, followed by a temperature scan from 200 to 725 °C at a specified heating rate. We note that longer purge times have no effect on the reaction or the results reported. Heating rates of 3, 5, 10, and 20 K/min were used. For the reaction of aluminum particles with oxygen, the mass of each sample was measured both before and after each run using an analytical balance in order to calculate the fraction of aluminum that reacted based on sample weight gain (as described later).

The obtained heat flow responses were corrected using baseline subtraction, where the baseline was obtained by running the empty reference and sample pans. The temperature of the instrument was calibrated using zinc and potassium chromate under argon atmosphere. Heat flow was calibrated using potassium chromate.

Heat transfer effects are known to smear transitions in DSC scans, leading to broader transitions and a shift along the temperature scale [31]. Although the heat of reaction is obtained from the integrated heat flow and is not be affected by any smearing of the transition, peak temperatures and reaction rates can be affected. The temperature gradient in the sample can be estimated following the arguments of Chang [32] by

$$\Delta T\,(\mathrm{K}) \approx 0.5 \frac{L}{A\lambda} Q \tag{4}$$

where L is the sample thickness (assumed to be 1 mm), A the sample area (0.126 cm^2), λ the thermal conductivity, and Q is the maximum heat flow. The thermal conductivity of our oxide-coated aluminum nanoparticle samples can be estimated by first calculating the average thermal conductivity for an individual particle based on particle geometry and the thermal conductivities of aluminum ($\lambda_{Al} = 2.36\ W\,cm^{-1}\,K^{-1}$) and aluminum oxide ($\lambda_{Al_2O_3} = 0.3\ W\,cm^{-1}\,K^{-1}$) [33]:

$$\lambda_{\mathrm{particle}} = \frac{R_o}{(r_{Al}/\lambda_{Al}) + (t_{\mathrm{oxide}}/\lambda_{Al_2O_3})} \tag{5}$$

where R_o is the total particle radius, r_{Al} the radius of the aluminum core, and t_{oxide} is the oxide coating thickness. The effective thermal conductivity, λ_{eff}, of the powder can then be estimated by accounting for the void fraction using the Maxwell theory [34]:

$$\frac{\lambda_{\mathrm{eff}}}{\lambda_{\mathrm{particle}}} \approx 1 - \frac{3}{2}\phi \tag{6}$$

where ϕ is the void fraction in the sample. The thermal conductivities of the individual particles range from 0.78 to 1.4 $W\,cm^{-1}\,K^{-1}$, increasing with increasing particle diameter. Assuming a void fraction of 50%, the thermal conductivity of the samples ranges from 0.20 to 0.35 $W\,cm^{-1}\,K^{-1}$, again increasing with increasing diameter. Hence, Eq. (4) becomes $\Delta T \approx 0.002Q$ to $0.001Q$, for Q in milliwatts, with the prefactor decreasing with increasing particle size. Thermal gradients in the DSC samples are calculated to be less than 1 K for the Al/O_2 reaction and less than 0.1 K for the MIC reactions for all scan rates used in this work. This calculation is corroborated by the observation that our calculated apparent activation energies do not depend on conversion; this result and its implication are discussed in more detail later. Due to the small thermal gradients expected in these samples, no correction for heat transfer effects are made.

2.3. Thermogravimetric analyzer

Although the aluminum nanoparticles were stored under an argon atmosphere after delivery, they may have reacted with adventitious oxygen between the time that the supplier made the measurements of active aluminum content and our DSC experiments. Therefore, the active aluminum content was determined from mass uptake of oxygen using a Perkin-Elmer TGA-7. The mass of the TGA samples varied from 1 to 3 mg and a 25/75 mixture of O_2/Ar was used as the analysis gas. Experiments were performed for 960 min at 830 °C. The mass gain in the TGA is attributed to oxidation of active aluminum, as shown by the following reaction:

$$4Al + 3O_2 \rightarrow 2Al_2O_3 \tag{7}$$

The active aluminum content (c) can be calculated using the following equation:

$$c\,(\%) = \frac{108}{96}\,\Delta m\,(\%) \tag{8}$$

where Δm (%) is the percent mass gain in the TGA experiment. The calculated aluminum content based on our TGA measurements, as well as that reported by the supplier, is shown in Table 1. We reiterate that only minor changes in aluminum content (<3%) were observed over the course of our experiments due to storage in our laboratory.

2.4. Data analysis

For the reaction of the aluminum particles with oxygen, the fraction of aluminum that reacts to form Al_2O_3 during DSC experiments was determined from the fractional mass gain of the DSC sample (Δm), in an analogy to Eq. (8):

$$\text{Fraction Al reacted} = \frac{108}{96}\,\Delta m \tag{9}$$

The fraction of aluminum that reacts prior to melting can also be independently determined from the area of the melting endotherm (ΔH_m):

$$\text{Fraction Al reacted} = 1 - \frac{\Delta H_m}{\Delta H_{m,T}(r)} \tag{10}$$

where $\Delta H_{m,T}(r)$ is the total heat of melting expected if none of the active aluminum reacts prior to melting; the heat of melting is a function of particle radius (r). Although the bulk heat of fusion of aluminum is 396 J/g [33], the heat of fusion of aluminum nanoparticles decreases as the particle size decreases [3,35]; for example, $\Delta H_{m,T} = 320$ J/g for 40 nm radius passivated particles

[3]. Therefore, the heat of fusion for each particle was determined experimentally in this work, and the values are shown in Table 1; errors in $\Delta H_{m,T}$ are estimated to be 5% [3]. We note that the difference in the fraction of aluminum reacted using $\Delta H_{m,T}(r)$ rather than the bulk heat of fusion, $\Delta H_{m,T}(\infty)$, in Eq. (10) is small, ranging from 1 to 8%. As an aside, we note that the heat of fusion is predicted to decrease with particle size due to a relative increase in the surface energy as particles decrease [36]:

$$\Delta H_{m,T}(r) = \Delta H_{m,T}(\infty) - \frac{2\sigma_{sl}}{\rho_s r} \quad (11)$$

where σ_{sl} is solid–liquid interfacial energy and ρ_s is the solid phase density. However, experimental results in the literature for metallic nanoparticles [3,35,37] and for organic materials confined to the nanoscale [38] show a much larger depression in the heat of fusion than is predicted by Eq. (11); the reason for this discrepancy is not clear although explanations have been put forth [3].

For the reaction of aluminum with molybdenum trioxide, there is no mass change upon the reaction. Hence, the fraction of aluminum reacted during the DSC scan is obtained from the heat of the DSC melting peak, as expressed by Eq. (10).

The kinetics of solid-state reactions is usually described by the following equation:

$$\frac{d\alpha}{dt} = k(T) f(\alpha) = A \exp\left(\frac{E}{RT}\right) f(\alpha) \quad (12)$$

where α is the degree of conversion, t the time, T the temperature, $k(T)$ the temperature-dependent rate constant, which is usually described by the Arrhenius equation, A and E the pre-exponential factor and apparent activation energy, respectively, and $f(\alpha)$ is the reaction model for the certain reaction [39–42]. An isoconvensional method in which DSC scans are made at a series of heating rates can be used to obtain kinetic parameters, and the apparent activation can be obtained from the following equation [42]:

$$\ln(\beta) = c - \frac{E_\alpha}{RT_\alpha} \quad (13)$$

where c is a constant, β the heating rate, and E_α and T_α are the apparent activation energy and temperature at a specific degree of conversion α. The advantage of this isoconversional method is that the activation energy can be obtained without specifying a certain reaction model; therefore, this method is a model-free method [42].

3. Results and discussion

3.1. Aluminum/oxygen reaction

The results of the DSC studies focusing on the reaction of the aluminum nanoparticles with oxygen (Al/O_2 reaction) are discussed first since they will provide insight into the more complex oxidation reactions of the MIC materials. The effect of aluminum particle size on the reactivity of Al/O_2 reaction is demonstrated in Fig. 1, where DSC scans are shown for the 52 nm broad size distribution sample (105 nm weight-average diameter), the 43 nm narrow size distribution sample, and the 3 μm Al particles at a heating rate of 3 K/min under an a 25/75 O_2/Ar atmosphere. The heat flows are normalized by the aluminum content in the samples in order to make a valid comparison. Fig. 1 shows that there is a large exothermic reaction peak present for the nanoparticles prior to the aluminum melting peak at 660 °C due to the oxidation of aluminum by oxygen, whereas for the micrometer-size material, only a small exotherm is present prior to melting. The onset temperature for oxidation is also dramatically reduced for the nanopowders. In addition, compared with micrometer-size sample, the melting peaks for the nano-sized samples are considerably smaller, suggesting that more aluminum in the nanopowders reacted in the oxidation process prior to melting. Hence, the reactivity of aluminum nanoparticles is considerably higher than that of the micrometer-size sample. Qualitatively similar results were reported by Mench et al. [4] in their comparison of Alex aluminum nanopowder and micrometer-size aluminum particles by differential thermal analysis (DTA). The effect of particle size distribution is also very striking in Fig. 1, with the 52 nm broad size distribution sample showing higher reactivity than the 43 nm narrow size distribution sample even though the average particle size is larger for the broad size distribution sample; this finding will be discussed in more detail subsequently.

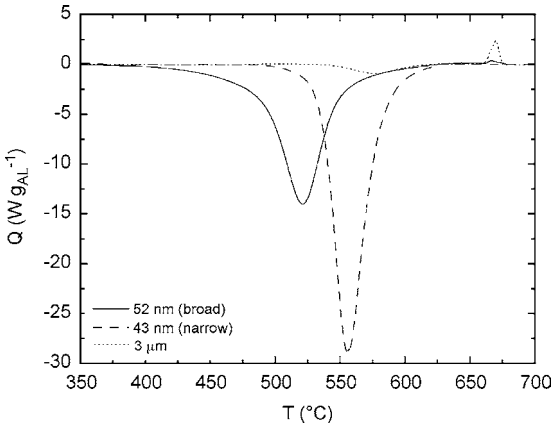

Fig. 1. DSC heat flow per gram of active aluminum as a function of temperature for the Al/O_2 reaction showing the effect of the size and size distribution of the aluminum nanoparticles. Results are shown for a broad size distribution sample having an average diameter of 52 nm (with a weight-average diameter of 105 nm), a 42 nm narrow size distribution sample, and a 3 μm sample. The DSC scans were performed at 3 K/min under 25/75 O_2/Ar atmosphere.

For the data shown in Fig. 1, the fraction of aluminum that reacts prior to melting can be calculated either from the mass gain of the DSC sample obtained by weighing the sample before and after the DSC experiment or from the area of the melting peak, using either Eq. (9) or (10), respectively. The results for all the samples including nanoparticles with both narrow and broad size distributions and micrometer-size particles are shown in Fig. 2 for DSC scans at 5 K/min as a function of reciprocal weight-average particle diameter. The fraction of aluminum that reacts prior to melting agrees between the two methods of calculation and increases with decreasing particle size leveling off for samples smaller than approximately 100 nm. For the 3 μm sample,

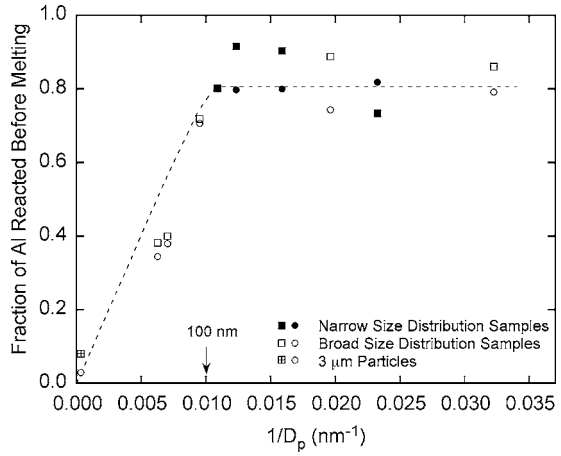

Fig. 2. Fraction of aluminum reacted prior to Al melting in the Al/O_2 reaction as a function of the reciprocal of the weight-average particle diameter for nanoparticles with both narrow and broad size distributions and for a micrometer-size sample. Results are based on DSC scans made at a heating rate of 5 K/min. Circles represent the results calculated from the mass gain of the sample, and squares represent the results calculated from the aluminum melting peak using the size-dependent heat of fusion. The dashed line is only intended to show the trend in the data.

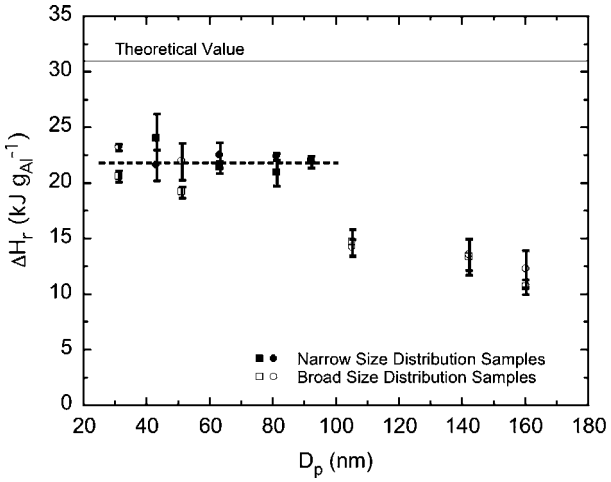

Fig. 3. Heat of reaction for the Al/O_2 as a function of weight-average particle diameter. The values plotted and error bars are the average and standard deviation, respectively, of the heat of reaction obtained at various heating rates. The circles represent the results based on the fraction of aluminum calculated from mass gain, and the squares represent the results based on the fraction of aluminum reacted calculated from the size of the aluminum melting peak using the size-dependent heat of fusion. The solid line indicates the bulk heat of reaction for Al/O_2. The dashed line is only intended to show the trend in the data for samples below 100 nm.

the fraction of aluminum that reacts prior to melting is less than 10%, whereas for particles of approximately 100 nm, the value increases to 80% and does not appear to increase further for smaller particles. Note that if the number-average particle size instead of weight-average size were used for the samples having broad distribution, the trend of the data would be obscured, confirming the importance of using the weight-average size. In this study, the effect of heating rate on the fraction of aluminum reacted prior to melting was also investigated. The fraction of aluminum that reacts prior to melting decreases by approximately 5% at 10 K/min and increases by approximately 5% at 3 K/min compared to the results shown for a 5 K/min heating rate; this is as expected since at higher heating rates, the samples have less time to react, and vice versa at lower heating rates. However, the trend for the fraction of aluminum that reacts prior to melting as a function of particle size is the same for all heating rates investigated.

The heat of reaction for the Al/O_2 reaction (ΔH_R) can be determined from the area of the exothermic reaction peak (shown in Fig. 1) coupled with knowledge of the amount of aluminum that reacted (Fig. 2). The results are shown in Fig. 3 as a function of the weight-average particle diameter for aluminum nanoparticles with both broad and narrow size distributions. At particle sizes less than approximately 100 nm, the heat of reaction is 23 kJ/g_{Al}, 75% of the theoretical value (31 kJ/g_{Al}) [43]. For particle sizes larger than 100 nm, the heat released per gram of aluminum reacting unexpectedly decreases with increasing particle size. We emphasize that the value reported is per gram of aluminum reacted. Our results for the smallest particles are consistent with work by Jones and co-workers [13] in which a value of approximately 22 kJ/g_{Al} was obtained for Alex aluminum nanoparticles by TG/DTA. We note that the heating rate has no effect on the heat of reaction values, and the data shown in Fig. 3 are the average and standard deviation of all the values obtained at different heating rates; i.e., although the fraction of aluminum reacted depends on heating rate, the heat of reaction per gram of aluminum reacted does not. In addition, the length of the purge prior to the DSC scan did not affect our results indicating that the lowered heats are not due, for example, to adventitious air or nitrogen in the samples. Although it may seem surprising that the heat of reaction for the nanoparticles is smaller than that for bulk aluminum, perhaps such a result is not so unexpected given the lack of understanding of material behavior at the nanoscale, including, for example, the large reductions in the heat of fusion observed at the nanoscale [3,35,37,38].

The size distribution of the nanopowders impacts their reactivity, as was shown in Fig. 1, where the exothermic reaction peak for the broad size distribution sample is shifted to lower temperatures by about 50 °C relative to that of the narrow size distribution sample, even though the broad size distribution sample has a larger average particle size. In an attempt to quantify the differences in reactivity, the onset and peak temperatures for all of the samples are shown in Fig. 4 as a function of weight-average particle diameter for DSC scans at 5 K/min. [We note that the onset temperature is defined as the temperature at which the extrapolated descending peak slope intersects with the baseline; this value depends on heating rate and is a measure of reactivity, not a direct measure of the temperature at which reaction begins.] As shown in Fig. 4, the onset and peak temperatures are lower for the broad size distribution samples than for the narrow size distribution samples, but in neither case do they depend strongly on particle size. The onset temperatures for samples with broad size distributions is approximately 505 °C, about 50 °C lower than those samples with narrow size distributions. For the micrometer-size sample, the onset temperature is close to that of the samples with narrow size distributions. The

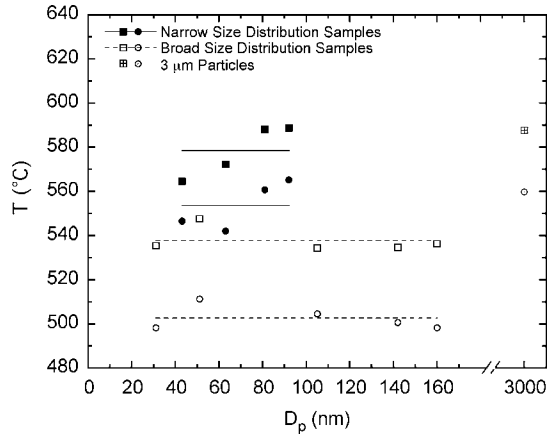

Fig. 4. Onset and peak temperatures as a function of weight-average particle diameter for the reaction of Al/O_2 for DSC scans at 5 K/min. Circles represent the onset temperature, and squares represent the peak temperature. The dashed and solid lines are only intended to show the trends in the data.

trend is the same for peak temperature, i.e., samples with broad size distributions have a lower peak temperature than those with broad size distributions. Both the onset temperature and peak temperatures are affected by the heating rates as expected, with the values being an average of 10 K lower for 3 K/min scanning rates and an average of 10 K higher for 10 K/min scanning rates. The results indicate that broad size distribution samples are more reactive than the narrow size distribution samples. This may be attributable to the presence of more small nanoparticles in a broad size distribution sample, which then may enhance the reactivity of the entire mixture.

The maximum oxidation rate per gram of aluminum reacted (Q_{max}), which is determined by the heat flow rate at the exotherm peak (with heat flow normalized by the total mass of aluminum of the sample) is plotted against weight-average particle diameter for all the samples studied in Fig. 5. With increasing particle size, the maximum oxidation rate decreases from approximately 55 W/g_{Al} for the particle of 60 nm diameter to 2 W/g_{Al} for the micrometer-size sample. Although Fig. 4 shows that the onset and peak temperatures are affected by the size distribution and not affected by the size of the particles, Fig. 6 indicates that the

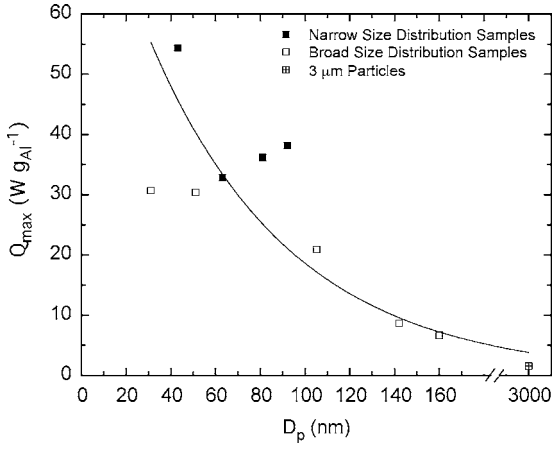

Fig. 5. Maximum reaction rate as a function of weight-average particle size for the reaction of Al/O_2 for DSC scans at 5 K/min.

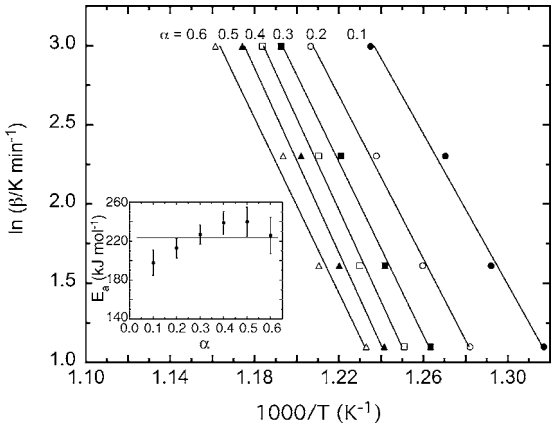

Fig. 6. Natural logarithm of the heating rate vs. the reciprocal temperature for various conversions, α, for the Al/O_2 reaction of the 25 nm sample having a broad size distribution. The lines show the best linear fits from which E_α is obtained. The dependence of E_α on conversion is shown in the inset with error bars indicating the standard error from the fit. The horizontal line in the inset indicates the average value of E_α for all conversions.

maximum reaction rate is strongly dependent on the particle size and not on the size distribution. Other parameters to characterize reactivity of aluminum nanoparticles besides onset and peak temperatures include the specific heat release (J/g) and maximum oxidation rate (g/min) in TG-DTA experiments [5,6,13] and the maximum self-heating rate (R_{max}) in ARC experiments [5,13]. Consistent with our data, other researchers have shown that aluminum nanoparticles ranging from 130 to 280 nm have considerably higher values of specific heat release [6] compared with 80 μm aluminum particles, and that with decreasing particle size, the values increase [6]. On the other hand, the onset temperatures for these aluminum nanoparticles from TG-DTA experiments show no large differences within the range studied [6], also in agreement with our DSC data. It is important to recognize that different measures of reactivity give different results, e.g., some measures indicate that particle size is important and that size distribution is unimportant, whereas others indicate the opposite. It is clear that a full description of reactivity requires multiple characterization methods.

The kinetics of the reaction of the aluminum nanoparticles with oxygen was studied using the isoconvensional method to calculate the apparent activation energy. Fig. 6 shows the natural logarithm of the heating rate (β) as a function of the reciprocal temperature at which a given conversion was obtained during the DSC scan for the 25 nm particle; the conversion α ranges from 0.1 to 0.6 since the final conversion for a heating rate of 20 K/min was less than 70%. From the slope of the ln β versus $1/T$ curves, E_α is calculated using Eq. (13). The results are shown in the inset of Fig. 6, where E_α is plotted as a function of conversion with the error bars giving the standard error from the fits. The values of E_α are not statistically different; this is consistent both with a simple reaction mechanism and with the absence of significant thermal gradients [44].

The average values for E_α and standard deviations are shown in Fig. 7 as a function of weight-average particle diameter. For all of the nanoparticles studied, the activation energies are in the range of 200–300 kJ/mol. This is in reasonable agreement

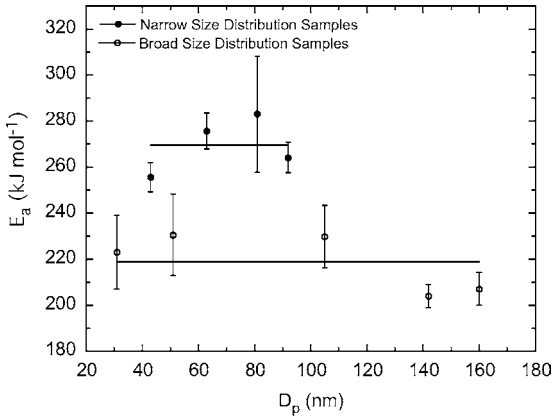

Fig. 7. Apparent activation energy calculated using the isoconversional method vs. particle size for the Al/O_2 reaction. The values plotted and error bars are the average and standard deviations, respectively, of the activation energies obtained at different conversions. The lines are only intended to show the trends in the data.

with literature values: a value of 164 kJ/mol was reported for oxidation of aluminum nanoparticles synthesized by gas condensation using TGA [18]; an average value of 254 kJ/mol was obtained by DSC and TGA experiments for oxidation of Alex aluminum nanoparticle [12]; also for Alex particles, a value of 225 kJ/mol was reported using DTA experiments [10]. From Fig. 7, we can also see that the apparent activation energies for particles with narrow distributions are slightly higher than those with broad distributions. For the aluminum nanoparticles with broad size distributions, the apparent activation energies are in the range of 220 ± 20 kJ/mol, whereas for those with narrow size distributions, the apparent activation energies are in the range of 270 ± 20 kJ/mol.

3.2. Aluminum/molybdenum trioxide MIC reaction

The effect of aluminum nanoparticle size on the reactivity of the Al/MoO_3 MIC reaction is also studied using DSC experiments. Fig. 8 shows a comparison of DSC scans run at 5 K/min for the MIC samples containing 52 nm and 3 μm aluminum particles, respectively. For the MIC sample containing 52 nm aluminum particles, there is a large exothermic peak followed by a small aluminum melting peak, whereas for the sample containing micrometer-sized aluminum, there is only a small exothermic peak followed by a large melting peak. Fig. 8 suggests that reducing aluminum particle size can significantly increase the reactivity of the Al/MoO_3 MIC, similar to the results shown in prior figures for the reaction of aluminum with oxygen. However, there are poignant differences between the MIC reaction and Al/O_2 reaction. First, the scale for heat flow for the reaction with the argon/oxygen mixture is over 10 times greater in Fig. 1 than for the MIC reaction shown in Fig. 8. In addition, the MIC reaction appears to be somewhat more complex with several peaks often observed in the temperature range from 250 to 600 °C. The apparent complexity may be due in part to the scale of the heat flow in Fig. 8 relative to Fig. 1; heat evolved due to reactions of the aluminum with adsorbed O_2 or H_2O or due to the phase change of aluminum oxide (Al_2O_3) from the amorphous to the crystalline state during temperature scan [24,45,46] may not be noticeable in Fig. 1 due to the scale of the heat flow. DSC experiments were performed separately for aluminum nanoparticles and for MoO_3 under argon atmosphere, and the results suggest some heat evolution for the aluminum nanoparticles either due to adsorbed O_2 or to the phase change of the Al_2O_3, whereas for MoO_3, no obvious peaks exist during the entire temperature scan.

The fraction of aluminum that reacts prior to melting is determined from the area of the melting endothermic peak, which reflects the amount of aluminum left in the sample. Fig. 9 shows the fraction of aluminum reacted prior to melting for DSC scan at 5 K/min as a function of reciprocal of the weight-average particle size calculated using the modified bulk heat of fusion. Compared with the sample containing micrometer-sized aluminum particles, the samples containing nano-sized aluminum particles are considerably more reactive; for example, 70% of the aluminum reacts in the MIC reaction for the 30 nm particles, whereas only

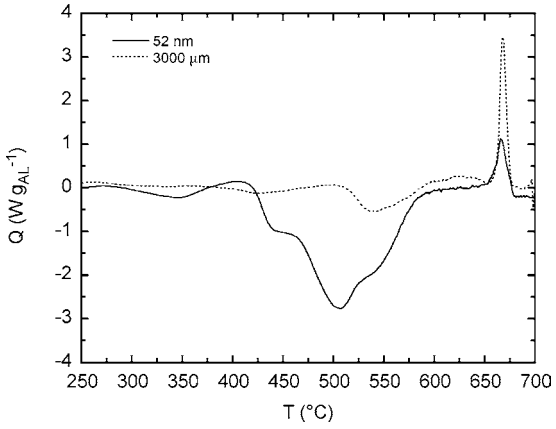

Fig. 8. DSC heat flow per gram of active aluminum as a function of temperature for the Al and MoO_3 MIC reaction showing the effect of aluminum particle size. The DSC scans were performed at 5 K/min under argon atmosphere.

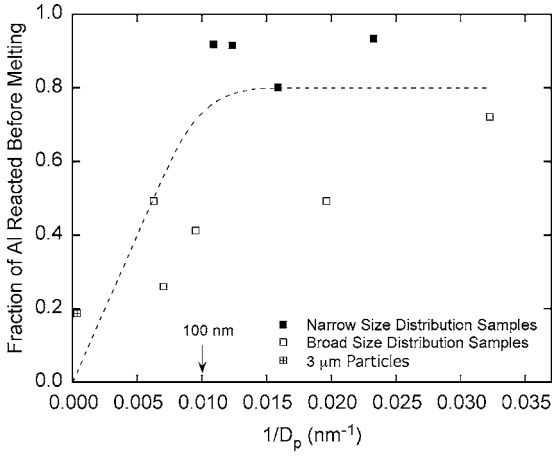

Fig. 9. Fraction of aluminum reacted prior to Al melting in the Al/MoO_3 MIC reaction as a function of the reciprocal of the weight-average aluminum particle diameter for nanoparticles and micrometer-size particle from DSC scans made at a heating rate of 5 K/min. The values are calculated from the size of aluminum melting peak using the size-dependent heat of fusion. The dashed line is only intended to show the trend in the data.

20% reacts for the 3 μm aluminum particles. For the aluminum nanoparticles with broad size distributions, the fraction of aluminum reacted appears to increase with decreasing particle size. For the narrow size distribution aluminum nanoparticles, which are all less than 100 nm, no significant differences exist for all four samples; this is consistent with the results for Al/O_2 reaction in which the fraction of aluminum that reacts before melting was independent of size for particles less than 100 nm. Note that since the actual equivalence ratio (ϕ) is lower than 1.2, as shown in Table 2, the fraction of aluminum reacted prior to melting may exceed 83%, the expected maximum for an equivalence ratio of 1.2. The effect of heating rate is significant for this reaction with the fraction of aluminum that reacts prior to melting decreasing with increasing heating rate; it is less than 35% for a heating rate of 10 K/min.

The heat of reaction for the Al/MoO_3 MIC reactions obtained from the integrated heat of the exothermic peak, is shown in Fig. 10, where the average heat of reaction is plotted against weight-average particle diameter. The heats of reaction obtained are considerably lower than the theoretical value (17 kJ/g_{Al}) [43], consistent with the results for the Al/O_2 reaction shown in Fig. 3 and the results of others [13]. For all the aluminum nanoparticles studied, the heats of reaction for MIC mixture are in the range of 6 ± 4 kJ/g_{Al}, approximately 35% of the theoretical value. The percentage of heat evolved per gram of aluminum reacting is much lower than that for the Al/O_2 reaction, and the results also show more scatter. Again, we emphasize that it is perhaps not surprising that the heat of reaction is lower than the bulk value given that a similar and, as yet, unexplained reduction is observed for the heat of fusion at the nanoscale.

The onset and peak temperatures for the Al/MoO_3 MIC reaction are shown in Fig. 11 for DSC scans at 5 K/min. The onset temperatures of the MIC samples containing aluminum nanoparticles with broad size distributions remain constant at approximately 460 °C, whereas those with narrow size distributions show onset temperatures at approximately 500 °C. The onset temperature for the sample containing micrometer-size aluminum particle is 518 °C, slightly higher than any samples having aluminum nanoparticles. The aluminum particle size appears to have no significant effect on the onset temperature for either narrow or broad size distributions for the Al/MoO_3 reaction, consistent with the results for the Al/O_2 reaction. The peak temperatures show a similar trend but with larger variations compared with the onset temperatures. The values of onset and peak temperatures increase with increasing heating rate and are approximately 10 K higher for a heating rate of 10 K/min.

The maximum reaction rate per gram of aluminum prior to aluminum melting for the Al/MoO_3 MIC reaction is shown in Fig. 12. With increasing aluminum particle size, the maximum oxidation rate appears to decrease with the trend being more obvious for the samples containing aluminum nanoparticles with broad size distributions. For the sample having micrometer-size aluminum, the maximum reaction rate is 0.6 W/g_{Al}, whereas for the sample having the smallest particles the value is approximately 10 times higher. The trend is similar to that for the Al/O_2 reaction although the rates are considerably lower.

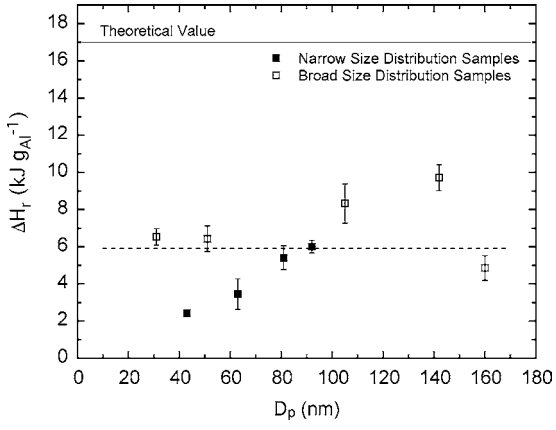

Fig. 10. Heat of reaction for the Al/MoO_3 MIC reaction as a function of weight-average aluminum particle diameter. The values plotted and error bars are the average and standard deviations, respectively, of the heat of reaction obtained at various heating rates. The solid line indicates the bulk heat of reaction, and the dashed line is only intended to show the trend in the data.

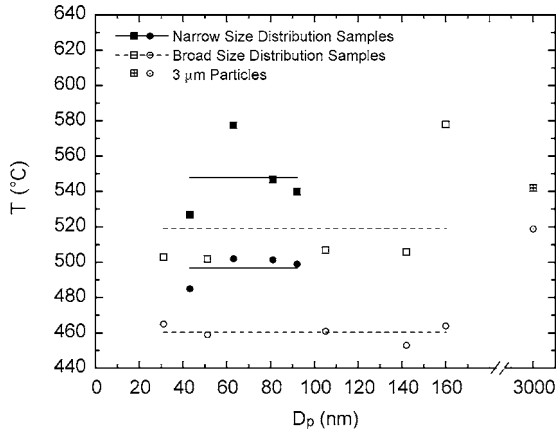

Fig. 11. Onset and peak temperatures as a function of weight-average aluminum particle diameter for the Al/MoO_3 MIC reaction for DSC scans at 5 K/min. Circles represent onset temperatures, and squares represent peak temperatures. The dashed and solid lines are only intended to show the trends in the data.

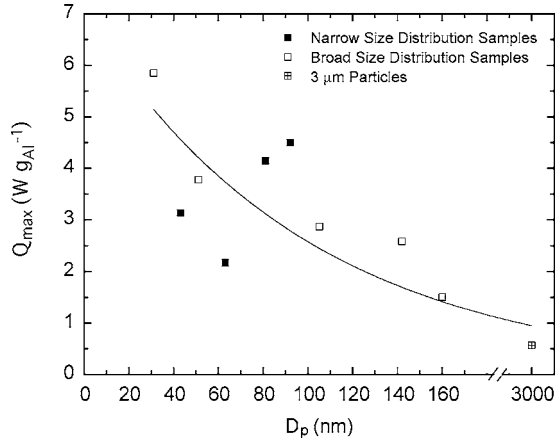

Fig. 12. Maximum reaction rate prior to melting as a function of weight-average aluminum particle size for the Al/MoO_3 MIC reaction for DSC scans at 5 K/min.

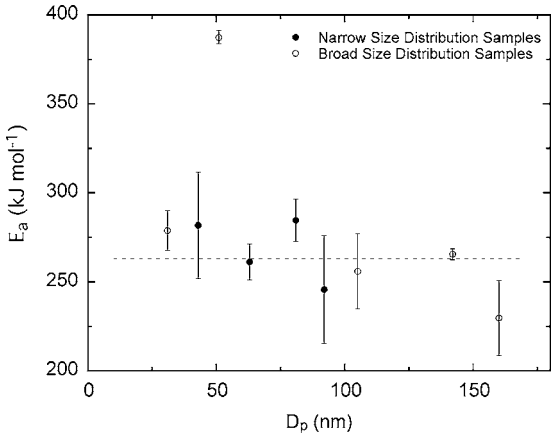

Fig. 13. Apparent activation energy calculated using the isoconversional method vs. weight-average aluminum particle diameter for the Al/MoO_3 MIC reaction. The values and error bars represent the average and standard deviation of the activation energy obtained at different conversions, respectively. The dashed line is only intended to show the trend in the data.

The apparent activation energy for the MIC reaction is also investigated using the isoconversional method. Fig. 13 shows the apparent activation energy versus weight-average particle diameter. Particle size seems to have no significant effect on the apparent activation energy for Al/MoO_3 reaction, with most samples having an apparent energy of 260 ± 20 kJ/mol, including both narrow and broad size distributions, although one sample shows a considerably higher activation energy for an unknown reason. For most of the samples, the value of apparent activation energy for Al/MoO_3 reaction is essentially the same as that for Al/O_2 reaction (260 ± 20 kJ/mol versus 240 ± 30 kJ/mol), suggesting that the two reactions have the same rate-limiting step.

4. Summary

The oxidation reactions of aluminum nanoparticles with oxygen and molybdenum trioxide were investigated using DSC. Both broad and narrow size distributions of aluminum nanoparticles have been investigated with the weight-average particle diameters ranging from 30 to 160 nm. The results show that for both Al/O_2 and Al/MoO_3 reactions, the aluminum nanoparticles reacts well before the melting of the aluminum compared with micrometer-size aluminum particle. The heats of reaction are lower than the theoretical values with the values ranging from 10 to 25 kJ/g_{Al} for the Al/O_2 reaction. The onset and peak temperatures for both Al/O_2 and Al/MoO_3 reactions are affected by the particle size distribution, and the temperatures for the narrow size distribution samples were approximately 50 °C higher than those for broad size distribution samples; no effect of particle size was observed for onset and peak temperatures. On the other hand, the maximum reaction rate for both reactions depends on particle size, and with decreasing particle size, the maximum reaction rate increases. The fact that some measures of reactivity depend on particle size and not on the size distribution, whereas other measures depend on size distribution and are independent of particle size, indicates the need to fully characterize reactivity using multiple characterization methods. The isoconversional method was used to calculate activation energies; for both the Al/O_2 Al/MoO_3 reactions, E_a ranges from 200 to 300 kJ/mol, suggesting the same rate-limiting step in these two reactions.

Acknowledgements

The authors gratefully acknowledge the financial support provided from the National Science Foundation DMR-0304640 (SLS) and the Army Research Office DAAD19-02-1-0214 (MLP).

References

[1] N. Ichinose, Y. Ozaki, S. Kashu, Superfine Particle Technol. (1992) 1–38.
[2] Ph. Buffat, J.-P. Borel, Phys. Rev. A 13 (1976) 2287–2298.
[3] J. Sun, Ph.D. Thesis, Texas Tech University, 2004;
J. Sun, S.L. Simon, in preparation.
[4] M.M. Mench, K.K. Kuo, C.L. Yeh, Y.C. Lu, Combust. Sci. Technol. 135 (1998) 269–292.
[5] D.E.G. Jones, R. Turcotte, R.C. Fouchard, Q.S.M. Kwok, A.M. Turcotte, Z.A. Qader, Propellants Explosives Pyrotech. 28 (2003) 120–131.
[6] A.P. Il'in, A.A. Gromov, G.V. Yablunovskii, Combust. Explosion Shock Waves 37 (2001) 418–422.
[7] A.P. Il'in, E.M. Popenko, A.A. Gromov, Y.Y. Shamina, D.V. Tikhonov, Combust. Explosion Shock Waves 38 (2002) 665–669.
[8] Y.S. Kwon, A.A. Gromov, A.P. Ilyin, Combust. Flame 131 (2002) 349–352.
[9] D.E.G. Jones, R. Turcotte, Q.S.M. Kwok, M. Vachon, L. Guindon, D. Lepage, V.Y. Gertsman, NATAS Proceedings, 2004.
[10] D.E.G. Jones, P. Brousseau, R.C. Fouchard, A.M. Turcotte, Q.S.M. Kwok, J. Therm. Anal. Calorim. 61 (2000) 805–818.
[11] C.E. Aumann, G.L. Skofronick, J.A. Martin, J. Vac. Sci. Technol. 13 (1995) 1178–1183.
[12] A. Tompa, R.F. Boswell, P. Skahan, C. Gotzmer, J. Therm. Anal. 49 (1997) 1161–1170.
[13] Q.S.M. Kwok, R.C. Fouchard, A.M. Turcotte, P.D. Lightfood, R. Bowes, D.E.G. Jones, Propellants Explosives Pyrotech. 27 (2002) 1–12.
[14] P. Brousseau, C.J. Anderson, Propellants Explosives Pyrotech. 27 (2002) 300–306.
[15] H. Ritter, S. Braun, Propellants Explosives Pyrotech. 26 (2001) 311–314.
[16] A. Dokhan, E. Price, J. Seitzman, R. Sigman, The ignition of ultra-fine aluminum in ammonium perclorate solid propellant flames, in: Paper AIAA-2003-4810 at the 39th AIAA/ASME/SAE/ASEE Joint Propulsion Conference, Huntsville, Al, July 20–23, 2003.
[17] M.E. Brown, S.J. Taylor, M.J. Tribelhorn, Propellants Explosives Pyrotechn. 23 (1998) 320–327.
[18] A. Pivkina, P. Ulyanova, Y. Frolov, Propellants Explosives Pyrotechn. 29 (2004) 39–48.
[19] W.L. Perry, B.L. Smith, C.J. Bulian, J.R. Busse, C.S. Macomber, R.C. Dye, S.F. Son, Propellants Explosives Pyrotechn. 29 (2004) 99–105.
[20] J.J. Granier, M.L. Pantoya, Laser ignition of nanocomposite thermites, Combust. Flame 138 (2004) 373–383.
[21] E.M. Hunt, K.B. Plantier, M.L. Pantoya, Acta Mater. 52 (2004) 3183–3191.
[22] M. Pantoya, S. Son, W. Danen, B. Jorgensen, B. Asay, J. Busse, J. Mang, Characterization of metastable intermolecular composites (MICs), in: A.W. Miziolek, S.P. Karna, J.M. Mauro, R.A. Vaia (Eds.), Defense Applications of Nanomaterials, ACS Symposium Series, vol. 891, Copyright American Chemical Society, 2005, pp. 227–240 (Chapter 16).
[23] D. Pesiri, C.E. Aumann, L. Bilger, D. BOoth, R.D. Carpenter, R. Dye, E. O'Neil, D. Shelton, K.C. Walter, J. Pyrotechn. 19 (2004) 19–31.
[24] M.A. Trunov, M. Schoenitz, X. Zhu, E.L. Dreizin, Combust. Flame 140 (2005) 310–318.

[25] M. Zhang, M.Y. Efremov, F. Schiettekatte, E.A. Olson, A.T. Kwan, S.L. Lai, T. Wisleder, J.E. Greene, L.H. Allen, Phys. Rev. B 62 (2000) 10548–10557.
[26] J.J. Granier, M.L. Pantoya, Combust. Theory Model. 8 (2004) 555–565.
[27] I. Levin, D. Brandon, J. Am. Ceram. Soc. 18 (8) (1998) 1995–2012.
[28] R.C. Weast, Handbook of Chemistry and Physics, CRC Press, 1973.
[29] B.S. Bockmon, M.L. Pantoya, S.F. Son, B.W. Asay, J.T. Mang, J. Appl. Phys. 98 (2005) 064903-1–064903-7.
[30] S. Turns, An Introduction To Combustion: Concepts and Applications, McGraw-Hill Companies, Inc., New York, 2000.
[31] J. Schawe, C. Schick, Thermochim. Acta 187 (1991) 335–349.
[32] S.S. Chang, Thermochim. Acta 178 (1991) 195–201.
[33] R.C. Weast, Handbook of Chemistry and Physics, 55th ed., CRC Press, 1974.
[34] K.W. Schlichting, N.P. Padture, P. Klemens, J. Mater. Sci. 36 (2001) 3003–3010.
[35] J. Eckert J., Y. Holzer, C.C. Ahn, Z. Fu, W.L. Johnson, Nanostruct. Mater. 2 (1993) 407.
[36] R. Defay, I. Prigogine, Surface Tension and Adsorption, John Wiley and Sons, 1967.
[37] K.M. Unruh, T.E. Huber, C.A. Huber, Phys. Rev. B 48 (1993) 9021–9027.
[38] C.L. Jackson, G.B. McKenna, J. Chem. Phys. 93 (1990) 9002.
[39] J.H. Flynn, L.A. Wall, J. Res. Natl. Bureau Standards A Phys. Chem. 70A (1966) 487–523.
[40] T. Ozawa, Bull. Chem. Soc. Jpn. 38 (1965) 1881–1886.
[41] J.H. Flynn, J. Therm. Anal. 34 (1988) 367–381.
[42] S. Vyazovkin, J. Comput. Chem. 22 (2001) 178–183.
[43] D.R. Stull, H. Prophet, JANAF Thermochemical Tables, second ed., NSRDS, 1971.
[44] S. Vyazovkin, J. Comput. Chem. 18 (1997) 393–402.
[45] J.M. McHale, A. Auroux, A.J. Perrotta, A. Navrotsky, Science 277 (1997) 788–790.
[46] L.P.H. Jeurgens, W.G. Sloof, F.D. Tichelaar, E.J. Mittemeijer, Thin Solid Films 418 (2002) 89–101.